Biophysical Journal
Article

Biophysical Society

Mechanism of Axonal Contractility in Embryonic *Drosophila* Motor Neurons In Vivo

Alireza Tofangchi,[1] Anthony Fan,[1] and M. Taher A. Saif[1,*]
[1]Department of Mechanical Engineering, University of Illinois at Urbana-Champaign, Urbana, Illinois

ABSTRACT Several in vitro and limited in vivo experiments have shown that neurons maintain a rest tension along their axons intrinsically. They grow in response to stretch but contract in response to loss of tension. This contraction eventually leads to the restoration of the rest tension in axons. However, the mechanism by which axons maintain tension in vivo remains elusive. The objective of this work is to elucidate the key cytoskeletal components responsible for generating tension in axons. Toward this goal, in vivo experiments were conducted on single axons of embryonic *Drosophila* motor neurons in the presence of various drugs. Each axon was slackened mechanically by bringing the neuromuscular junction toward the central nervous system multiple times. In the absence of any drug, axons shortened and restored the straight configuration within 2–4 min of slackening. The total shortening was ~40% of the original length. The recovery rate in each cycle, but not the recovery magnitude, was dependent on the axon's prior contraction history. For example, the contraction time of a previously slackened axon may be twice its first-time contraction. This recovery was significantly hampered with the depletion of ATP, inhibition of myosin motors, and disruption of actin filaments. The disruption of microtubules did not affect the recovery magnitude, but, on the contrary, led to an enhanced recovery rate compared to control cases. These results suggest that the actomyosin machinery is the major active element in axonal contraction, whereas microtubules contribute as resistive/dissipative elements.

INTRODUCTION

Numerous studies have shown that neurites actively respond to tensile forces by growing. Bray (1) demonstrated that neurites grow in length when towed at a controlled rate. Similarly, Pfister et al. (2) showed that axons are able to elongate to a thousand times their original length when simply subjected to a mechanical tension. The elongated axons retain their electrophysiological functions (3). These results are not surprising given the fact that neurites are coupled to the peripheral system, which can sometimes grow at a rapid rate (~3.45 cm/day in the case of the blue whale (4)) during early development. Recent experiments have shown that unperturbed neurons are also tensed (rest tension >0) in vitro (5) and in vivo (6), further supporting the stretch-growth theory.

Neurons also actively regulate and maintain their rest tension (7). For instance, chick sensory neurons subjected to slackening undergo shortening and restore their tension, in most cases to a level greater than the initial value, within 60–90 min (8). Similar behaviors are observed in chick forebrain neurites, but to a lesser degree (9). Likewise, contractile behavior is observed in axons that are previously subjected to a fairly large sustained strain. For example, upon removal of external forces, stretch-grown dorsal root ganglion neurons in rat pups contract at rates up to 6.1 μm/s and a rest tension is slowly restored within 20 min (10). We have also previously observed that *Drosophila* axons actively maintain a rest tension of 1–13 nN and axons that are made slackened become taut and restore a rest tension of similar magnitude in 10–30 min (11). Contraction is also observed in neurites that are surgically severed. Earlier, Shaw et al. (12) described how isolated axon segments in vitro often shorten after they are resected. A number of in vitro studies have also demonstrated similar shortening behavior of axons upon surgical incision (13–15). These results suggest that maintaining an intrinsic tension is an integral part of neural activities.

One study suggests that vesicle clustering in the presynaptic terminal of neuromuscular junctions (NMJs) in embryonic *Drosophila* is dependent on mechanical tension in the axons (6). Clustering decreases upon surgically severing the axon (intrinsic tension is compromised), but clustering is restored upon simply restoring the tension by stretching the severed axon. Further stretching the axon increases

Submitted April 21, 2016, and accepted for publication August 18, 2016.
*Correspondence: saif@illinois.edu
Alireza Tofangchi and Anthony Fan contributed equally to this work.
Editor: Charles Wolgemuth.
http://dx.doi.org/10.1016/j.bpj.2016.08.024

clustering by as much as 200% in 30 min (6). In addition, it has also been shown that mechanical tension modulates local and global vesicle dynamics in *Drosophila* neurons (16) and that acute brain slices "remember" the previously prescribed mechanical stretch and respond by showing hyperexcitability (17).

In this study, we address the question, what is the origin of tension in motor neuron axons? A surgically cleaned single-axon system in *Drosophila* enables us to simply bring the NMJs closer to the central nervous system (CNS). Typically, in the absence of any drug, the axons shorten, become taut, and regain tension. This cycle of slackening and straightening can be repeated multiple times, resulting in axons shortening by up to 40% of their original length in some embryos. The magnitude and rate of shortening are used as measures of contractility. We find that contractility decreases dramatically after myosin II knockdown and inhibition, and in the presence of actin-disrupting drugs. However, the rate of contractility is faster when microtubules (MTs) are disrupted. These observations suggest that the mechanical tension in *Drosophila* motor neurons is primarily generated by the actomyosin machinery.

MATERIALS AND METHODS

Culture and dissection of *Drosophila* embryos

Transgenic *Drosophila* (elav0-GAL4,UAS-gap::GFP) expressing green fluorescent protein (GFP) in neuronal membranes were used for the experiments. These flies were also crossed with homozygous UAS-zipRNAi flies (37480, Bloomington Stock Center, Bloomington, IN) to knock down *zipper* in neurons (18). Repo-GAL4 and UAS-mCD8::GFP flies (7415 and 32184, Bloomington Stock Center) were crossed to visualize glial membrane. Drosophila was cultured on standard grape agar plates at room temperature (23°C). For harvesting, the embryos were dechorionated with a 50/50 bleach/water solution for 2 min and then rinsed with deionized water (19). Embryos of stages 15–16—identified by gut morphology, CNS condensation, and time elapsed after egg laying—were placed on a double-sided tape attached to a glass coverslide. They were then incubated under insect saline solution before being devitellinized. The embryos were oriented such that the ventral nerve cord was closest to the glass surface, and a glass dissection needle was used to make a dorsal incision. The dissection was made from posterior to anterior along the embryo to remove the guts and lay the body walls down flat. Then the axons of the aCC motor neuron and the RP2 motor neuron, which comprise the intersegmental nerve, were isolated by gently removing other nearby sensory and motor neurons, as well as fat cells and muscle fibers around them. The NMJs of the aCC and RP2 neurons were not damaged during this process. In some cases, the axon of the RP2 neurons was also excised, leaving only the axon of the aCC neuron intact. In most cases, both axons were intact and we measured their combined response. Glass microneedles were fabricated using a Sutter Instruments (Novota, CA) laser-based micropipette/fiber puller.

Micromanipulator and imaging

Actuation of the microneedle (Fig. 1 *A*) was powered and controlled by an XYZ piezo-actuator (NanoPZ PZC200, Newport, Irvine, CA). Live imaging of the axon under the applied deformation was carried out on an inverted microscope (IX81, Olympus, Nashua, NH). An Andor Neo sCMOS camera cooled to −30°C was used to record images (Andor Technology, Belfast, United Kingdom) at 2 frames/s. Imaging parameters (e.g., light intensity, exposure time, gain, etc.) were kept constant during all experiments.

Axon compression and contraction measurement

To relax the axonal shaft, a microneedle tip was gently placed on the tissue embedding the NMJs (Fig. 1 *A*). The tissue was then pushed toward the CNS by 10–15% of the initial axon length. We traced the profile of the

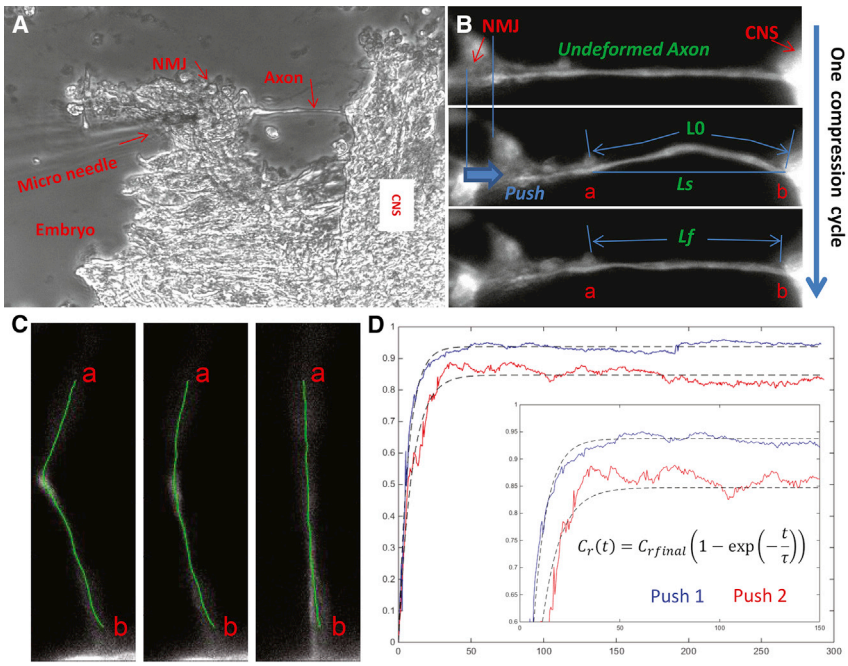

FIGURE 1 Experimental setup and data analysis methods. (*A*) Phase-contrast image of a dissected embryo. The axon is being pushed with the microneedle from its NMJ end. (*B*) The geometrical parameters are labeled on the fluorescent image of an axon undergoing a complete slackening cycle. (*C*) Path-length computation achieved by tracing the intensity centroid along the length of axons at different time points. (*D*) Contraction-factor-versus-time plot of an axon pushed twice. Dotted lines are least-square fits of the inset equation to the raw data. The inset plot provides an expanded look at the transient region. To see this figure in color, go online.

axon (Fig. 1 *C*) by getting the intensity centroid along the x axis for every position of y:

$$C(y) = \sum_{x=x_{\min}}^{x_{\max}} xI[x,y] \Big/ \sum_{x=x_{\min}}^{x_{\max}} I[x,y]. \quad (1)$$

The obtained C in Eq. 1 was then smoothed by its moving average over one-tenth of its total length. Path length was obtained by summing the euclidean distances between each point after smoothing. The symbols used for measuring axon contraction are listed in Box 1.

Drug treatments

Drugs used include 2-deoxyglucose and sodium azide for ATP depletion (20), ML-7 to inhibit myosin light-chain kinase (MLCK) (13), Y-27632 to inhibit myosin rho kinase (ROCK) (21), Latrunculin A (22,23), and cytochalasin D (24) for disruption of actin filaments, and Nocodazole and Colchicine to disrupt MTs (25); all stocks were from Sigma-Aldrich (St. Louis, MO). Dimethylsulfoxide (4-X, ATCC, Manassas, VA) was used as a solvent, tested to have no observable effect at low concentration. All drugs were diluted in Ca^{2+}/Mg^{2+}-free phosphate-buffered saline (PBS).

Immunofluorescence staining

The prepared embryos were fixed with 4% formaldehyde (28908, Fisher Scientific, Rockford, IL) for 15 min, permeabilized with 0.5% Triton X-100 (X100, Sigma-Aldrich) for 10 min, blocked in 5% bovine serum albumin (A9647, Sigma-Aldrich) for 10 min, conjugated with mouse anti-α-tubulin (1:100; A11126, Fisher Scientific) or mouse anti-repo (1:20; 8D12, DSHB, Iowa City, IA) for 60 min; tagged with Alexa 568 goat anti-mouse (1:200; A-11004, Fisher Scientific) for 30 min, and imaged with a scanning confocal microscope (LSM700, Carl Zeiss, Peabody, MA) afterward. Samples were rinsed with PBST (PBS with 0.1% Triton X-100) after each step. All steps were performed at room temperature. A brief extraction step was added before fixation in some of the MT-staining experiments to distinguish polymerized MTs from the soluble tubulin pool. Permeabilization was skipped in these instances.

RESULTS

Axons have robust contraction ability upon sustained loss of tension

We investigate 1) whether embryonic *Drosophila* axons are capable of generating contractile force after they undergo mechanically induced loss of tension, and 2) the dynamics of such contraction due to multiple successive compression cycles.

To remove tensile force in the axonal shaft, the axon was compressed from the NMJ side (Fig. 1 *A*), which caused the axon to buckle and become slack (Fig. 1 *B*). However, the axon exhibited gradual self-shortening (Fig. 1, *B* and *C*) and ultimately reached a stable straight configuration (Fig. 1 *D*) within 2–3 min (end of compression cycle 1/push 1). The degree of contraction for each axon in a cycle was characterized by the contraction factor, C_r, defined as,

$$C_r = \frac{\Delta L_f}{\Delta L_s} = \frac{L_0 - L_f}{L_0 - L_s}. \quad (2)$$

Here, $0 \le C_r \le 1$. $C_r = 0$ indicates no contraction ($L_0 = L_f$); $C_r = 1$ indicates full contraction ($L_f = L_s$, for nomenclature, see Fig. S2 *A* in the Supporting Material and Box 1). All embryos showed a high degree of contraction, with C_r = 0.90–0.95 in cycle 1. To investigate whether the shortened axons could further contract when subjected to another round of slackening, we examined the same axon for a second compression cycle (push 2) after 1 h ($\Delta T_1 = 1$ h). The axon reached a steady state and became fairly straight within 2–4 min, with C_r = 0.80–0.90. Finally, the same axon was pushed for the third cycle (push 3) after a half hour ($\Delta T_2 = 0.5$ h, Figs. 2 *A* and S2 *B*; Movie S1). Again, shortening occurred within 2–4 min with a C_r close to those in previous cycles. This was consistent among all six embryos examined (Fig. 2 *B*). Note that because the axon length decreased at the end of each compression cycle, the values of L_0, L_f, and L_s vary among compression cycles. It is also worth noting that the total compressive strain (based on L_0 in cycle 1 and L_f in cycle 3) exceeded 40% in some embryos, although axon length varied from 70 μm to 105 μm from embryo to embryo.

These results show the rapidity and robustness of axon shortening in response to multiple occasions of loss of tension. Results here will also serve as our control data in the later sections describing embryo subjection to various pharmaceutical treatments.

BOX 1 List of Symbols in the Axon Compression Experiment

L_0	Measured arc length of axon from point a to point b (Fig. 1 *B*) immediately after push
L_f	Measured arc length of axon from point a to point b 5 min after push
L_s	Straight-line distance between points a and b, ideal length of a taut axon
C_r	Contraction factor $\frac{\Delta L_f}{\Delta L_0} = \frac{L_0 - L_f}{L_0 - L_s}$ represents normalized magnitude of axonal contraction
τ	Time constant of axonal contraction by assuming a first-order decay
ΔT	Time interval between compression cycles.

Axon contraction shows exponential decay over time with less shortening rate in the second compression cycle

To study the dynamics of *Drosophila* axon contraction, we monitored time-lapsed images of axons and measured their instantaneous change of length over time (Fig. 1 *C*) during both the first and second compression cycles. The time-dependent contraction can be fitted to a first-order exponential equation as

$$C_r(t) = C_{r_{\text{final}}}\left(1 - e^{-\frac{t}{\tau}}\right), \quad (3)$$

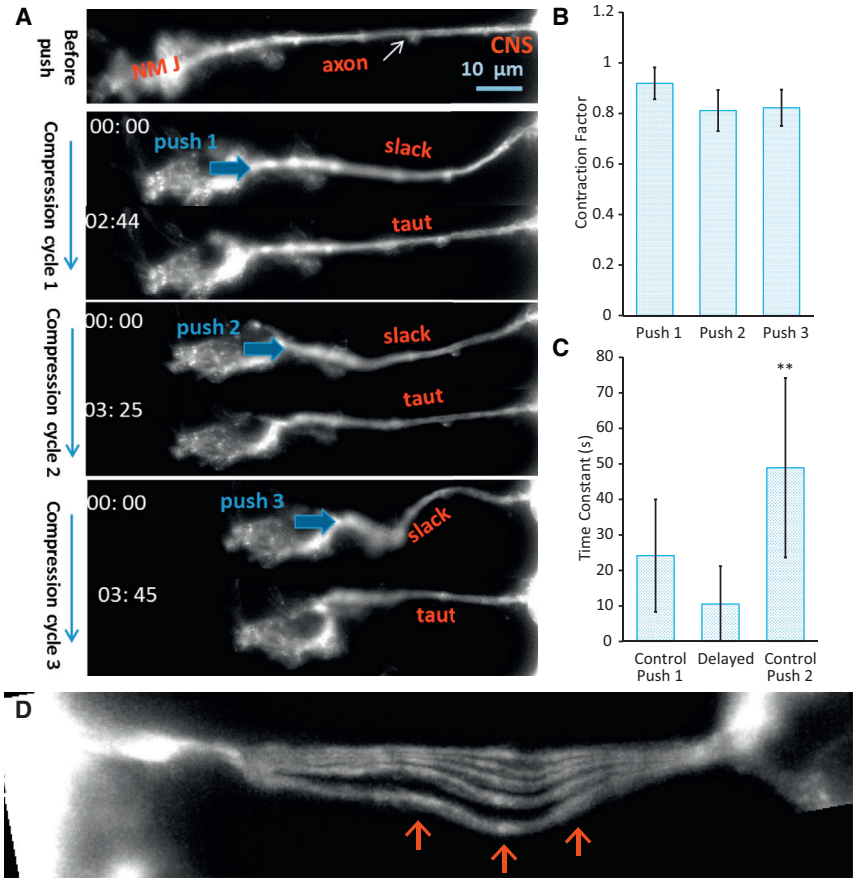

FIGURE 2 Axon shows robustness and nonlocalization in contraction. (*A*) Experimental images showing an axon contract during three consecutive slackening cycles. The contraction strain in each cycle is 10–15% of the initial length (L_0 in each cycle). Note that the axon contracts and becomes taut upon each push within 2–4 min. The total shortening is ~40% of the original length (L_0 in cycle 1). (*B*) C_r for each compression cycle, demonstrating robust axonal contractility ($n = 6$ in all groups). (*C*) Time constants of contraction for axons pushed (first time) immediately after surgical preparation, pushed (first time) 1 h after surgery, and pushed the second time 1 h after the first push ($n = 6$ in all groups). (*D*) The same axon overlaid at different time points—0, 10, 20, 30, and 50 s—after a push. Movements of fluorescence intensity features (*red arrows*) reveal a change in forcing direction along the length. All error bars indicate the standard deviation. To see this figure in color, go online.

where experimentally, $C_r(t) = ((L_0 - L(t))/(L_0 - L_s)), L(t)$ is the instantaneous length, and τ is the characteristic time constant (Fig. 1 *D*).

$C_{r_{\text{final}}}$ (reported simply as C_r in the previous section (Eq. 2)) and τ represent the two independent parameters characterizing the magnitude and rate, respectively, of axon contraction in a given compression cycle.

We found that all axons exhibited a generic exponential decay in shortening over time in both cycles (Fig. 1 *D*). We further analyzed the behavior by plotting $\ln(1 - (C_r(t)/C_{r_{\text{final}}}))$ as a function of time. Data from six randomly chosen axons show a linear dependence (Fig. S1). However, contractions in the first cycle, performed either immediately ($n = 6$) or 1 h ($n = 6$) after embryo preparation, had a faster rate of contraction (consistently among embryos) compared to the second cycle ($n = 6$, Fig. 2 *C*). The 1-h-delay experiment was done to assess any saline incubation effect. Note that the C_r was similar in both cycles and seemed to be largely independent of τ.

Contraction is distributed along the length of the axon

The magnitude (C_r) and rate (τ) of contraction quantify the bulk response of the axons. To gain insight into the source of contraction, such as which cytomachinery is involved, we quantified the local dynamics of the axons along their lengths. First, we overlaid the profiles of the same axon at different time points during contraction (Fig. 2 *D*) and traced the positions of a few markers along the length (*red arrows*). If the contractile units are localized to a specific region, for example, the NMJ, all the fluorescence markers will move toward the NMJ when tensed—with displacement magnitude decreasing as we move away from the NMJ. The different markers did not move toward the same end of the axon. This implies that the source of contraction is distributed and is not localized to the NMJ or CNS side.

Contraction behavior of axons subject to drug treatment

To explore the mechanism of axonal contraction, we investigated the contraction response of axons subjected to various pharmaceutical drugs. Each drug has a potent ability to impair/disrupt specific cellular activity/structure in axons, as discussed in the next sections. Results from the previous sections (Figs. 2 *B* and S2 *B*) serve as the control group. Fig. S2 *C* provides a detailed schematic of the procedures. Briefly, all drugs were added immediately after the

completion of push 1 and allowed to sit for $\Delta T = 1$ h, similar to control procedures, before push 2 commenced.

Axons contraction is active and requires metabolic energy for contraction

To investigate whether the process of axon contraction is active and hence requires metabolic energy, the embryos were treated ($n = 6$) with combined 2Deoxyglucose (60 mM, 1 h) and sodium azide (20 mM) to deplete ATP (20). As expected in the first compression cycle, the axon contracted with $C_r = 0.80 \pm 0.10$, whereas in the second compression cycle, the contraction factor noticeably dropped to $C_r = 0.13 \pm 0.09$ (Fig. 3 *A*). Thus, ATP inhibitory reagent significantly impaired axon contraction, suggesting that axonal contractility is an active process supported by metabolic energy. We note that ATP depletion may lead to impairment of myosin II motors and major actin filament depolymerization, both of which are verified in the next sections to lead to loss of tension and contractility of the axon.

Myosin II contributes to force generation in axons through MLCK and ROCK pathways

In the first set of experiments, we used transgenic embryos that expressed UASzipRNAi in neurons to knock down *zipper* (18), the gene encoding nonmuscle mysoin II in *Drosophila* ($n = 7$). We observed significant inhibition of axon contraction ($C_r = 0.31 \pm 0.13$), indicating that myosin II mediates axon contraction (Fig. 3 *B*; Movie S2).

To further identify the molecular pathways by which myosin II is activated in axons, we separately treated the embryos with reagents ML-7, an inhibitor of MLCK (13) ($n = 6$, 225 μM, 1 h), and Y-27632, an inhibitor of ROCK (21) ($n = 6$, 110 μM, 1 h). Both ML-7 and Y-27632 reduced axon contraction in the second cycle (Fig. S3, *A* and *B*), with $C_r = 0.36 \pm 0.20$ and 0.33 ± 0.17, respectively (Figs. 3 *C* and S3 *C*). Drug effects have saturated at the concentration reported here (Fig. S3, *C* and *D*). Contraction was also significantly reduced at lower concentrations (70 μM and 35 μM for ML-7 and Y-27632, respectively (Fig. S3, *C* and *D*)) (26,27). These results together indicate that both MLCK and ROCK pathways contribute to myosin-based contraction and force-generating machinery in live *Drosophila* axons.

Axon contraction stops upon disruption of F-actin/cortical actin

Myosin motors employ actin filaments to generate intracellular tension. Therefore, if myosin II is indeed involved in axonal contractility, then disruption of actin filaments should also result in loss of contractility. To examine this hypothesis, embryos were separately treated with cytochalasin D (50 μg/mL, $n = 6$) and Latrunculin A (31 μM, $n = 6$), potent reagents that disrupt actin filaments (22–24). As is evident in Fig. 4 *A* and Movie S3, both cytochalasin D and Latrunculin A significantly impaired the ability of axons to contract, as characterized by the reduced values of $C_r = 0.18 \pm 0.12$ and $C_r = 0.16 \pm 0.13$, respectively, in the second cycle.

Disruption of MTs accelerates contraction dynamics

Since the axonal shaft is abundant with MTs, we ask whether the MT has any direct role in axonal contraction. To address this question, the embryos were treated

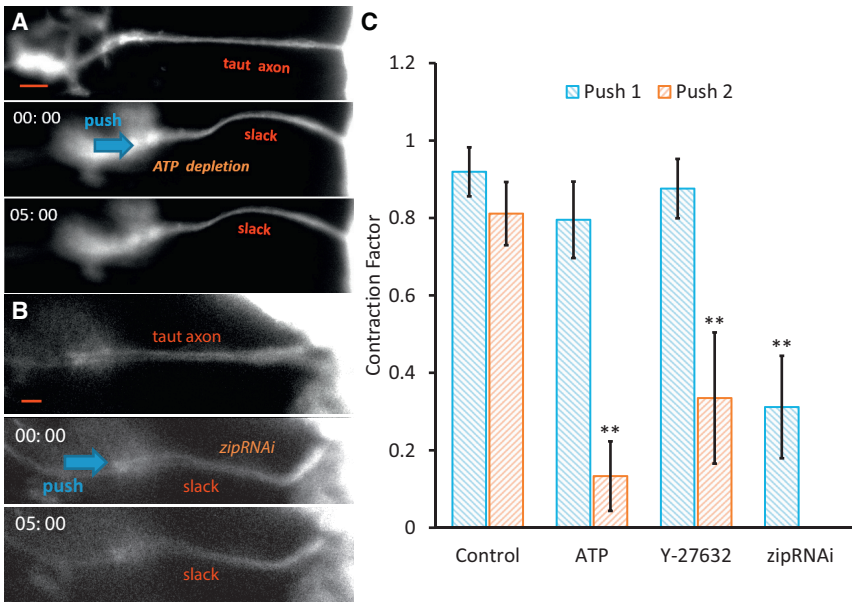

FIGURE 3 Effect of pharmaceutical and genetic disruption of nonmuscle myosin II. (*A*) Axon contraction stops when ATP is depleted by treating embryos with 2Deoxyglucose and sodium azide. This indicates that axon contraction is active and needs metabolic energy ($n = 6$). Similarly, axons stop to contract when nonmuscle myosin II is knocked down by (*B*) zipRNAi ($n = 7$). (*C*) Summary of results suggesting that myosin II is involved in active force generation in *Drosophila* axons. Note that no drugs are used in the control cases. Scale bar, 10 μm. All error bars indicate the standard deviation. To see this figure in color, go online.

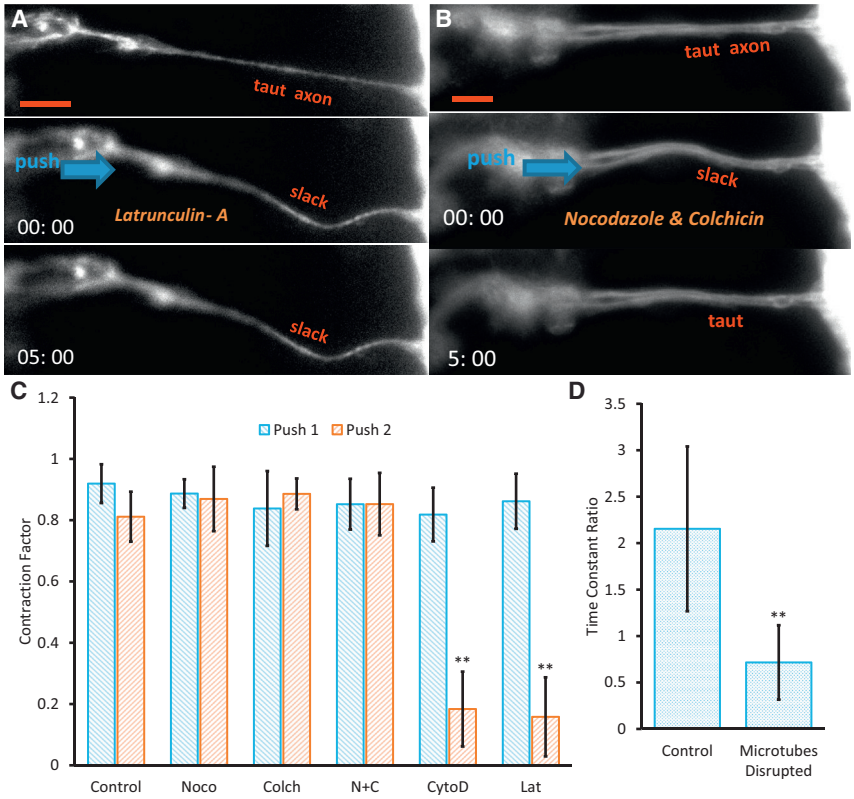

FIGURE 4 Effect of pharmaceutical cytoskeleton disruption. (*A*) Axon contraction is significantly inhibited when the embryo is treated with cytochalasin D ($n = 6$) and Latrunculin A ($n = 6$). (*B*) The axon contraction factor remains unaffected, as compared to control cases, when embryos are treated with Nocodazole ($n = 4$) and Colchicin ($n = 4$) both independently and combined ($n = 6$). (*C*) The summary of results shows a significant decrease in axon contraction when actin structures are disrupted, whereas the axon contraction factor remains insensitive to disruption of MTs. (*D*) The time constant ratio (τ_2/τ_1) is significantly reduced ($n = 5$), indicating that contraction is happening at a faster rate, when MTs are disrupted. No drugs were used in the control cases. Scale bar, 10 μm. All error bars indicate the standard deviation. To see this figure in color, go online.

separately and simultaneously with Nocodazole (15 μg/mL) and Colchicine (200 μM), potent drugs to destabilize microtubules (15,28). After drug treatments, axons maintained a high $Cr = 0.87 \pm 0.11$ ($n = 4$, Nocodazole), 0.89 ± 0.05 ($n = 4$, Colchicine), and 0.85 ± 0.10 ($n = 6$, Nocodazole + Colchicine) in the second cycle, similar to the control data, indicating that axon contraction factor alone is insensitive to MT disruption (Fig. 4, *B* and *C*; Movie S4). Disruption of MTs resulted in tubulin beading along the axon and a reduction in α-tubulin intensity (Fig. S4), as typically observed in MT disruption experiments (28). Time constant comparison reveals that the MT disruption expedites the contraction, i.e., the axon contracts faster, and this is reflected in τ. The ratio of the time constants (contraction time constant of push 2 divided by that of push 1, $R\tau = (\tau_2/\tau_1)$) with and without microtubule disruption is $(R\tau_{(\mu T-)}/R\tau) \simeq (1/3)$ (Fig. 4 *D*), suggesting that MTs act as resistive and dissipative elements in axonal contraction.

DISCUSSION

It has long been known that neurons cultured on petri dishes generate tension. Recent studies show that in vivo axons of embryonic *Drosophila* also generate tension (6). More importantly, this tension seems to play a critical role in clustering neurotransmitter vesicles at the presynaptic terminal. Such clustering is essential for neurotransmission. Here, we seek for the origin of tension in neurons in embryonic flies by applying a series of cytoskeletal disruptive drugs. Our key conclusion is that actomyosin machinery is primarily involved in the contractility of axons of embryonic motor neurons. This contractility results in tension in the axons. We have the following remarks.

Glial cells possibly influence axon contraction

Physiology studies (29) have shown that glial ensheathment, continuous along the nerve, is complete at stage 17. The embryos that we worked with (stages 15–16) also showed a high degree of glial ensheathment, as evident by immunofluorescence staining targeting repo, a gene that is expressed only in glial cells (Fig. S5). However, possibly because of the immature coupling between glial cells and axons, all of our cleaned preparations showed minimal ensheathment along the shaft of the axons (Fig. S5). The axons were still able to contract and generate tension in the absence of glial cells along their length. It is therefore unlikely for the glial populations to influence the rest tension and the contraction factors reported in this work. However, it is possible that glial cells also contribute to axon contractility locally providing more resistance to buckling, which in turn influences the bulk time constant (Fig. 2 *C*) and the profile after deformation and during the contraction process (Fig. 2 *D*).

Actomyosin machinery is important in generating axon rest tension in vitro and in vivo

In vitro studies revealed the role of cytoskeletal structure and motor protein activity in axon contractility in different types of neurons. For instance, disruption of F-actin eliminates retraction of neurites (13,30), and depolymerization of the actin network leads to a significant reduction in the rest tension in axons (31). The role of actin in axonal contractility in embryonic *Drosophila*, in which actin was observed to actively participate in contraction dynamics (Fig. 4, *A* and *C*), seems to be consistent with the in vitro studies.

Motor proteins also have a significant role in force generation and motility of axons. For example, it has been shown that retractions in chick sensory neurons (30), Neuro–2A neurites (21), and DRG neurons (13) are significantly dependent on myosin II. These results agree with our observations that myosin II plays a major role in contraction dynamics; axon contraction was significantly impaired when myosin II was downregulated by RNAi and inhibited using pharmaceutical reagents (Fig. 3). This, combined with our results on actin disruption, strongly suggests that the interplay of actomyosin machinery drives the fast active contraction of slackened axons. It is also conceivable that the actin network serves as a force conduit along the axonal shaft. It can sustain and transmit both external force (31) and internally generated tension (by myosin motors, as shown in this study), and hence, once it is disrupted, contractility significantly drops in axons.

MTs participate by sliding, breaking, and densifying

The profile of buckling in our experiments was rarely of mode I and was usually a combination of multiple modes. This leads us to believe that the observed deformation profile is driven by the MTs, known to couple with surrounding cytoskeleton to buckle at higher modes to withstand compressive load (32). Under actomyosin contraction, the buckled MTs are thought to slide against each other, possibly influenced by tau proteins (33), leading to axon shortening. This allows the slackened axon to straighten and build up tension (11). Dynein motors might also be actively resisting the contraction (34). The time evolution of axon contraction in each cycle is analogous to that of a system modeled by a first-order decay equation (Fig. 1 *D*), suggesting the presence of resistive/dissipative elements (35) and supporting the hypothesis of MT sliding (36). Breaking of MTs might occur at high compression rate/magnitude as well (25). The rate at which they reassemble may influence the contraction dynamics. It is worth noting that such reassembling processes usually occur over a much longer timescale of axonal shortening, i.e., 40 min, compared to what we observe here (25). The subsequent reorganization and reassembling of MTs can further lead to a formation of a denser filamentous network upon axon shortening, which could explain the slower dynamics (higher time constant) in push 2 in our experiment. We showed that the time constant increase was reverted, i.e., shortening was expedited, when MTs were disrupted, supporting the hypothesis. Others have also shown that MTs counterbalance tensile forces along the F-actin in vitro. For instance, disruption of MTs in axons leads to an increase in rest tension (15,31), and destabilization or stabilization of MTs resulted in enhanced or retarded recovery rate, respectively, of dynamically stretched axons (25).

Force can mediate actin polymerization to scaffold synaptic vesicles

Contraction of slack axons along their entire length (Fig. 2 *D*) and the exponential time dependence of contraction (Figs. 1 *D* and S1) lead us to believe that axonal contractility results from a continuous network of cortical actin filaments (37) rich in myosin motors, but that the contraction is hindered by a frictional component originating from the central network of other cytoskeleton filaments, dominated by MTs. This is summarized in Fig. 5 *A*.

Tension is known to facilitate actin polymerization (38), and a loss of tension could lead to actin disassembly. It is thus possible that the self-generated tension sustains the actin network, especially farther downstream in the actin-rich presynaptic terminal, to provide a scaffold for synaptic vesicle clustering, which has been shown to be sensitive to all actin (39), myosin (18), and tension (6) disruption.

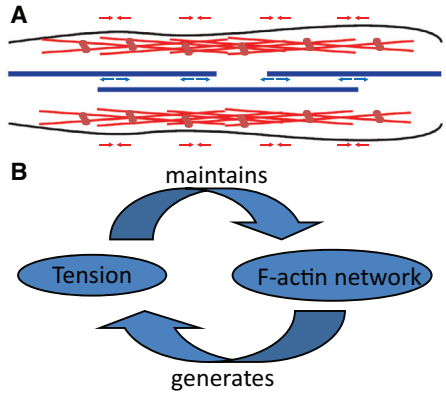

FIGURE 5 Schematic of a possible mechanism in force generation and contraction. (*A*) Cartoon schematic of a possible cytoskeleton configuration with cortical actomyosin network (*red network*) generating tension along the axon and microtubules (*blue strands*) resisting the contraction and providing support actively through molecular motors and/or passively through cross-linking proteins. (*B*) A possible loop mechanism is shown in which the actin network is stabilized by the tension it generates. Such a stable network may facilitate neurotransmitter vesicle clustering at the synapse, as well as other biological processes. To see this figure in color, go online.

Tension can influence stretch-sensitive ion channels

Maintaining tension might be vital for the functionality of ion channels. It has been argued that all ion channels are mechanosensitive—a large enough stress will induce conformational change in ion channels, which would lead to an increase/decrease in their activation energy barrier for conductance (40). Thus, it is conceivable that the tension generated by actomyosin machinery might serve as a signal for the ion channels. The latter in turn may influence polymerization of cytoskeletal components and motor activity by regulating their ion transport. Thus, the channels and the actomyosin machinery may act as a feedback-loop system, maintaining the rest tension and resulting in an optimal condition for neuronal function.

Tension can promote efficient wiring

It has been suggested that cortical folding in the cerebral cortex of large mammals could be driven by intrinsic axonal tension to pack the most neurons in a confined space, i.e., efficient wiring (41). Several efforts have been attempted to (dis)prove this hypothesis (42,43). Most experimental results suggest that intrinsic tension does not cause cortical folding, but no evidence has so far been presented against its role in efficient wiring.

As is evident from previous experiments (6,44), neurons respond to mechanical stimuli. However, a neuron, like any long wire, can only sense mechanical signal efficiently when it is tensed. The ultimate role of tension homeostasis in neurons may not merely be limited to growth, as is conventionally understood, but might be related to various neuronal functions, including axonal transport and synaptic transmission and excitability.

SUPPORTING MATERIAL

Five figures and four movies are available at http://www.biophysj.org/biophysj/supplemental/S0006-3495(16)30746-9.

AUTHOR CONTRIBUTIONS

A.T., A.F., and T.S. designed research. A.T. and A.F. performed research. A.T., A.F., and T.S. analyzed data. A.T., A.F., and T.S. wrote the article. All authors read and reviewed the article.

ACKNOWLEDGMENTS

We thank Wylie Ahmed and Jagannathan Rajagopalan for helpful discussion and comments on the manuscript and the Smith-Bolton group at the University of Illinois for fly food and helpful instructions on the RNAi experiments.

This work was supported by grants from the National Institutes of Health (NINDS NS063405-01) and the National Science Foundation, Science and Technology Center on Emergent Behaviors in Integrated Cellular Systems (EBICS; CBET-0939511, CMMI 1300808, DGE 1144245, and DGE 0965918).

REFERENCES

1. Bray, D. 1984. Axonal growth in response to experimentally applied mechanical tension. *Dev. Biol.* 102:379–389.
2. Pfister, B. J., A. Iwata, …, D. H. Smith. 2004. Extreme stretch growth of integrated axons. *J. Neurosci.* 24:7978–7983.
3. Pfister, B. J., D. P. Bonislawski, …, A. S. Cohen. 2006. Stretch-grown axons retain the ability to transmit active electrical signals. *FEBS Lett.* 580:3525–3531.
4. Lockyer, C. 1981. Growth and energy budgets of large baleen whales from the Southern Hemisphere. *In* Mammals in the Seas, vol. 1, document 41, *3*. Fisheries Department, FAO, pp. 379–487.
5. Heidemann, S. R., and R. E. Buxbaum. 1990. Tension as a regulator and integrator of axonal growth. *Cell Motil. Cytoskeleton.* 17:6–10.
6. Siechen, S., S. Yang, …, T. Saif. 2009. Mechanical tension contributes to clustering of neurotransmitter vesicles at presynaptic terminals. *Proc. Natl. Acad. Sci. USA.* 106:12611–12616.
7. O'Toole, M., P. Lamoureux, and K. E. Miller. 2015. Measurement of subcellular force generation in neurons. *Biophys. J.* 108:1027–1037.
8. Dennerll, T. J., P. Lamoureux, …, S. R. Heidemann. 1989. The cytomechanics of axonal elongation and retraction. *J. Cell Biol.* 109:3073–3083.
9. Chada, S., P. Lamoureux, …, S. R. Heidemann. 1997. Cytomechanics of neurite outgrowth from chick brain neurons. *J. Cell Sci.* 110:1179–1186.
10. Loverde, J. R., V. C. Ozoka, …, B. J. Pfister. 2011. Live imaging of axon stretch growth in embryonic and adult neurons. *J. Neurotrauma.* 28:2389–2403.
11. Rajagopalan, J., A. Tofangchi, and M. T. A Saif. 2010. *Drosophila* neurons actively regulate axonal tension in vivo. *Biophys. J.* 99:3208–3215.
12. Shaw, G., and D. Bray. 1977. Movement and extension of isolated growth cones. *Exp. Cell Res.* 104:55–62.
13. Gallo, G. 2004. Myosin II activity is required for severing-induced axon retraction in vitro. *Exp. Neurol.* 189:112–121.
14. George, E. B., B. F. Schneider, …, M. J. Katz. 1988. Axonal shortening and the mechanisms of axonal motility. *Cell Motil. Cytoskeleton.* 9:48–59.
15. Joshi, H. C., D. Chu, …, S. R. Heidemann. 1985. Tension and compression in the cytoskeleton of PC 12 neurites. *J. Cell Biol.* 101:697–705.
16. Ahmed, W. W., T. C. Li, …, T. A. Saif. 2012. Mechanical tension modulates local and global vesicle dynamics in neurons. *Cell. Mol. Bioeng.* 5:155–164.
17. Fan, A., K. A. Stebbings, …, T. Saif. 2015. Stretch induced hyperexcitability of mice callosal pathway. *Front. Cell. Neurosci.* 9:292.
18. Seabrooke, S., X. Qiu, and B. A. Stewart. 2010. Nonmuscle Myosin II helps regulate synaptic vesicle mobility at the *Drosophila* neuromuscular junction. *BMC Neurosci.* 11:37.
19. Budnik, V., M. Gorczyca, and A. Prokop. 2006. Selected methods for the anatomical study of *Drosophila* embryonic and larval neuromuscular junctions. *Int. Rev. Neurobiol.* 75:323–365.
20. Sheetz, M. P., N. L. Baumrind, …, A. L. Pearlman. 1990. Concentration of membrane antigens by forward transport and trapping in neuronal growth cones. *Cell.* 61:231–241.
21. Wylie, S. R., and P. D. Chantler. 2003. Myosin IIA drives neurite retraction. *Mol. Biol. Cell.* 14:4654–4666.
22. Spector, I., N. R. Shochet, …, Y. Kashman. 1989. Latrunculins—novel marine macrolides that disrupt microfilament organization and affect cell growth: I. Comparison with cytochalasin D. *Cell Motil. Cytoskeleton.* 13:127–144.

23. Lunn, J. A., H. Wong, …, J. H. Walsh. 2000. Requirement of cortical actin organization for bombesin, endothelin, and EGF receptor internalization. *Am. J. Physiol. Cell Physiol.* 279:C2019–C2027.
24. Cooper, J. A. 1987. Effects of cytochalasin and phalloidin on actin. *J. Cell Biol.* 105:1473–1478.
25. Tang-Schomer, M. D., A. R. Patel, …, D. H. Smith. 2010. Mechanical breaking of microtubules in axons during dynamic stretch injury underlies delayed elasticity, microtubule disassembly, and axon degeneration. *FASEB J.* 24:1401–1410.
26. Willoughby, L. F., T. Schlosser, …, A. M. Brumby. 2013. An in vivo large-scale chemical screening platform using *Drosophila* for anti-cancer drug discovery. *Dis. Model. Mech.* 6:521–529.
27. Wong, R., L. Fabian, …, J. A. Brill. 2007. Phospholipase C and myosin light chain kinase inhibition define a common step in actin regulation during cytokinesis. *BMC Cell Biol.* 8:15.
28. Ahmad, F. J., C. J. Echeverri, …, P. W. Baas. 1998. Cytoplasmic dynein and dynactin are required for the transport of microtubules into the axon. *J. Cell Biol.* 140:391–401.
29. Banerjee, S., and M. A. Bhat. 2008. Glial ensheathment of peripheral axons in *Drosophila*. *J. Neurosci. Res.* 86:1189–1198.
30. Ahmad, F. J., J. Hughey, …, P. W. Baas. 2000. Motor proteins regulate force interactions between microtubules and microfilaments in the axon. *Nat. Cell Biol.* 2:276–280.
31. Dennerll, T. J., H. C. Joshi, …, S. R. Heidemann. 1988. Tension and compression in the cytoskeleton of PC-12 neurites. II. Quantitative measurements. *J. Cell Biol.* 107:665–674.
32. Brangwynne, C. P., F. C. MacKintosh, …, D. A. Weitz. 2006. Microtubules can bear enhanced compressive loads in living cells because of lateral reinforcement. *J. Cell Biol.* 173:733–741.
33. Ahmadzadeh, H., D. H. Smith, and V. B. Shenoy. 2014. Viscoelasticity of tau proteins leads to strain rate-dependent breaking of microtubules during axonal stretch injury: predictions from a mathematical model. *Biophys. J.* 106:1123–1133.
34. Roossien, D. H., K. E. Miller, and G. Gallo. 2015. Ciliobrevins as tools for studying dynein motor function. *Front. Cell. Neurosci.* 9:252.
35. Bernal, R., F. Melo, and P. A. Pullarkat. 2010. Drag force as a tool to test the active mechanical response of PC12 neurites. *Biophys. J.* 98:515–523.
36. Suter, D. M., and K. E. Miller. 2011. The emerging role of forces in axonal elongation. *Prog. Neurobiol.* 94:91–101.
37. Xu, K., G. Zhong, and X. Zhuang. 2013. Actin, spectrin, and associated proteins form a periodic cytoskeletal structure in axons. *Science.* 339:452–456.
38. Courtemanche, N., J. Y. Lee, …, E. C. Greene. 2013. Tension modulates actin filament polymerization mediated by formin and profilin. *Proc. Natl. Acad. Sci. USA.* 110:9752–9757.
39. Kuromi, H., and Y. Kidokoro. 1998. Two distinct pools of synaptic vesicles in single presynaptic boutons in a temperature-sensitive *Drosophila* mutant, shibire. *Neuron.* 20:917–925.
40. Sachs, F. 2010. Stretch-activated ion channels: what are they? *Physiology (Bethesda).* 25:50–56.
41. Van Essen, D. C. 1997. A tension-based theory of morphogenesis and compact wiring in the central nervous system. *Nature.* 385:313–318.
42. Xu, G., P. V. Bayly, and L. A. Taber. 2009. Residual stress in the adult mouse brain. *Biomech. Model. Mechanobiol.* 8:253–262.
43. Xu, G., A. K. Knutsen, …, L. A. Taber. 2010. Axons pull on the brain, but tension does not drive cortical folding. *J. Biomech. Eng.* 132:071013.
44. Chen, B. M., and A. D. Grinnell. 1995. Integrins and modulation of transmitter release from motor nerve terminals by stretch. *Science.* 269:1578–1580.

Biophysical Journal, Volume *111*

Supplemental Information

Mechanism of Axonal Contractility in Embryonic *Drosophila* Motor Neurons In Vivo

Alireza Tofangchi, Anthony Fan, and M. Taher A. Saif

List of Figures

S1 Log-linear plot of contraction dynamics of six randomly chosen axons. Sets of experimental data are colored in solid lines. Corresponding best linear fits are graphed in dotted lines. 3

S2 Cartoon Schematics. (A) Graphical representation of various notation used. (B) Procedures of control experiments. (C) Procedures of pharmaceutical experiments. . 4

S3 Axon contraction inhibited by ML-7 (A) and Y-27632 (B). Effect of ML-7 (C) and Y-27632 (D) at approximately 67% & 33% of the concentration reported in the main text. N=6 in all cases. All error bars in standard deviation. Note that ML-7 at the applied concentration may lead to the inhibition of PKA, PKC, and other pathways. 5

S4 DIC, anti-α-tubulin, and neuronal-membrane-bound-GFP composite images with (A) and without (B) drug. Expanded images of microtubules morphology with (C) and without (D, reduced image gain by one-eighth due to saturation) drug. (E-J) Images obtained with a brief extraction step before fixation. Anti-α-tubulin and neuronal-membrane-bound-GFP composite images with (E, G, & I) and without (F, H, & J) drug. The composite images are separated into the two channels indicating the presence of polymerized microtubules (G & H) and neuronal membrane (I & J). Same imaging conditions applied unless otherwise noted. 6

S5 Glial cells visualizations, through staining (A-B) and crossing (C-F), show high degree of glial ensheatment of uncleaned axon, and minimal ensheathment along the axon shaft of cleaned axon. (A) DIC and anti-repo composite image of preparation. Cleaned axon on the left. (B) Anti-repo channel of A. (C & E) Phase and glial-membrane-bound-GFP composite images at 2 different focal planes. Cleaned axon on the right. (D & F) Glial-membrane-bound-GFP channel of C & E respectively. . . 7

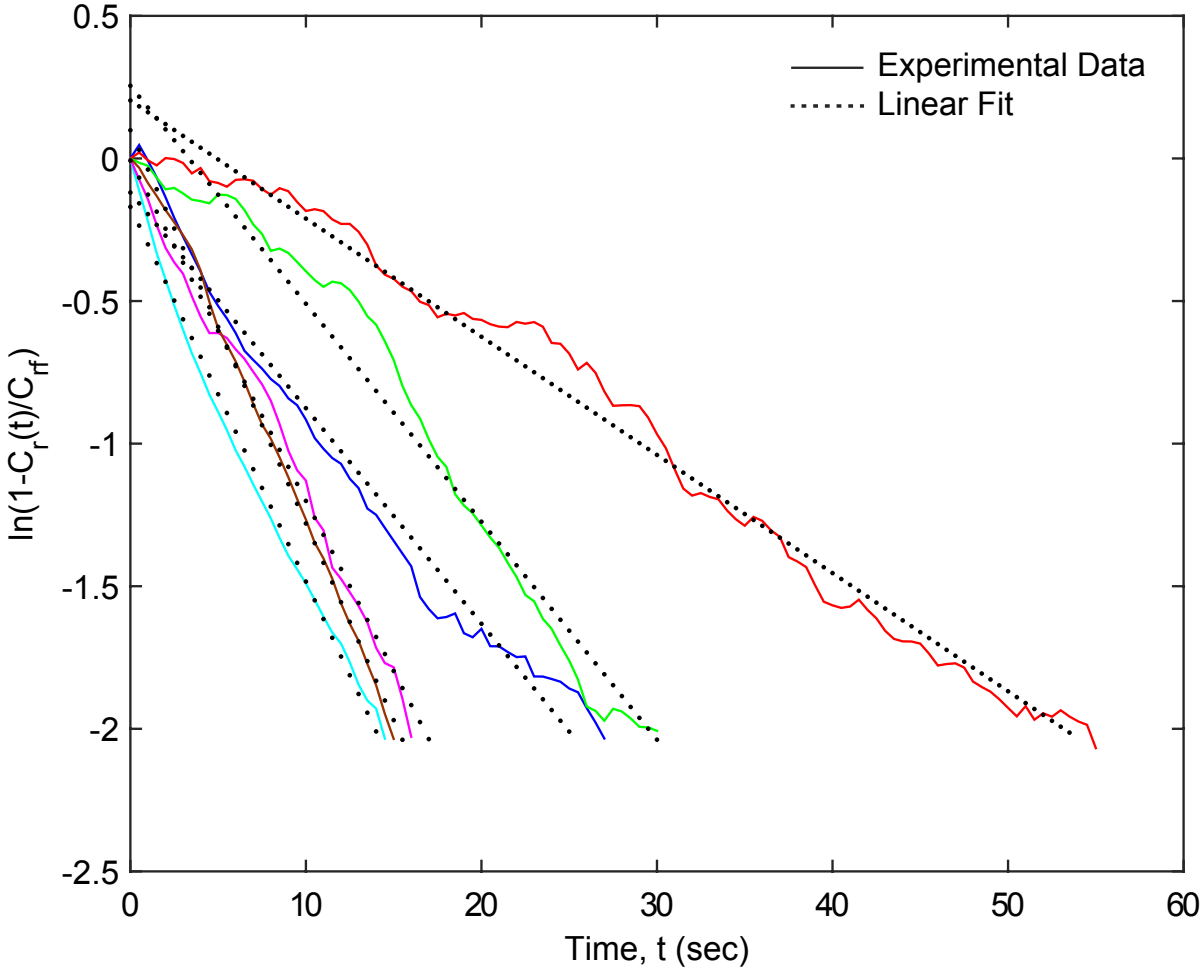

Figure S1: Log-linear plot of contraction dynamics of six randomly chosen axons. Sets of experimental data are colored in solid lines. Corresponding best linear fits are graphed in dotted lines.

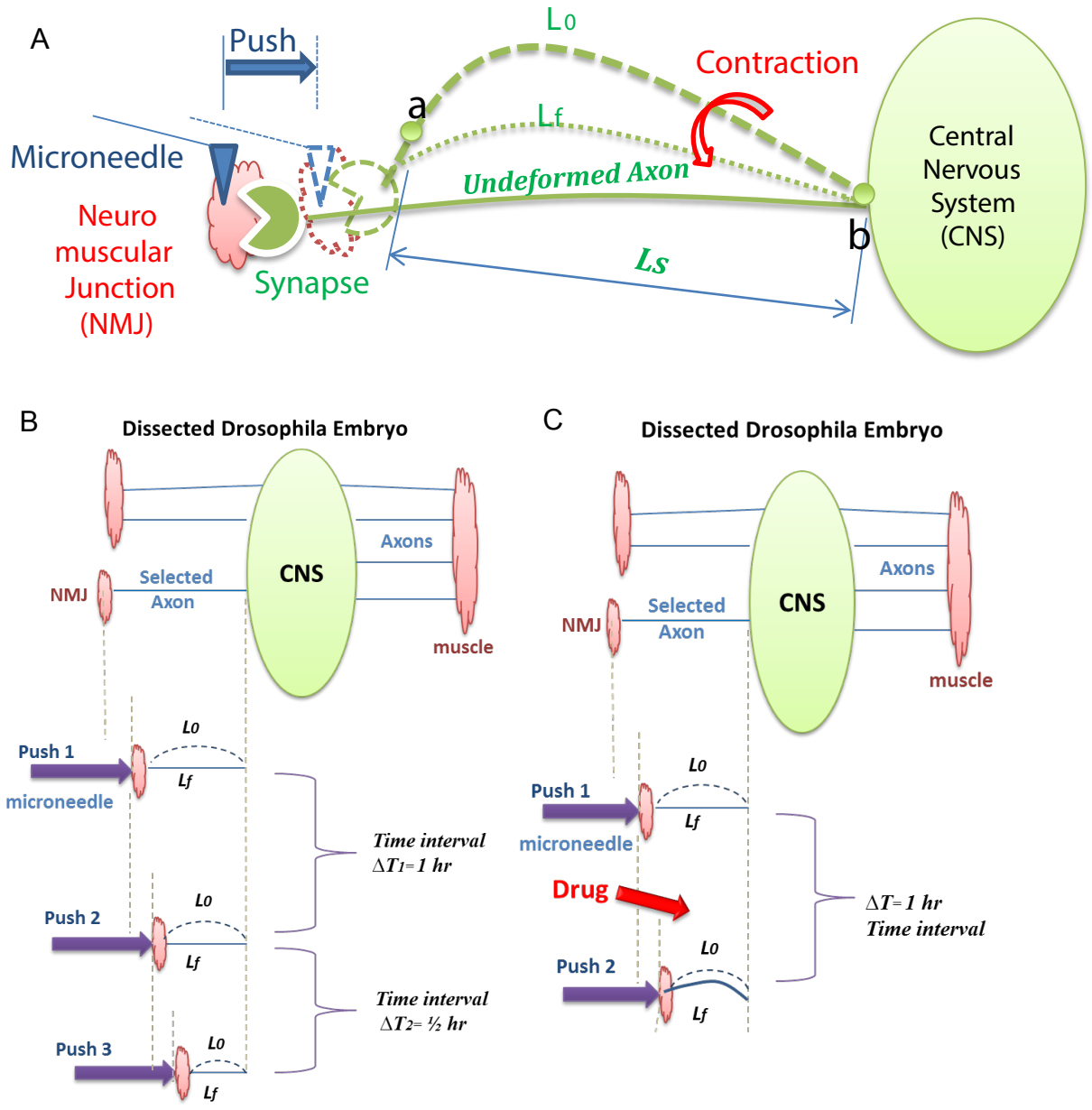

Figure S2: Cartoon Schematics. (A) Graphical representation of various notation used. (B) Procedures of control experiments. (C) Procedures of pharmaceutical experiments.

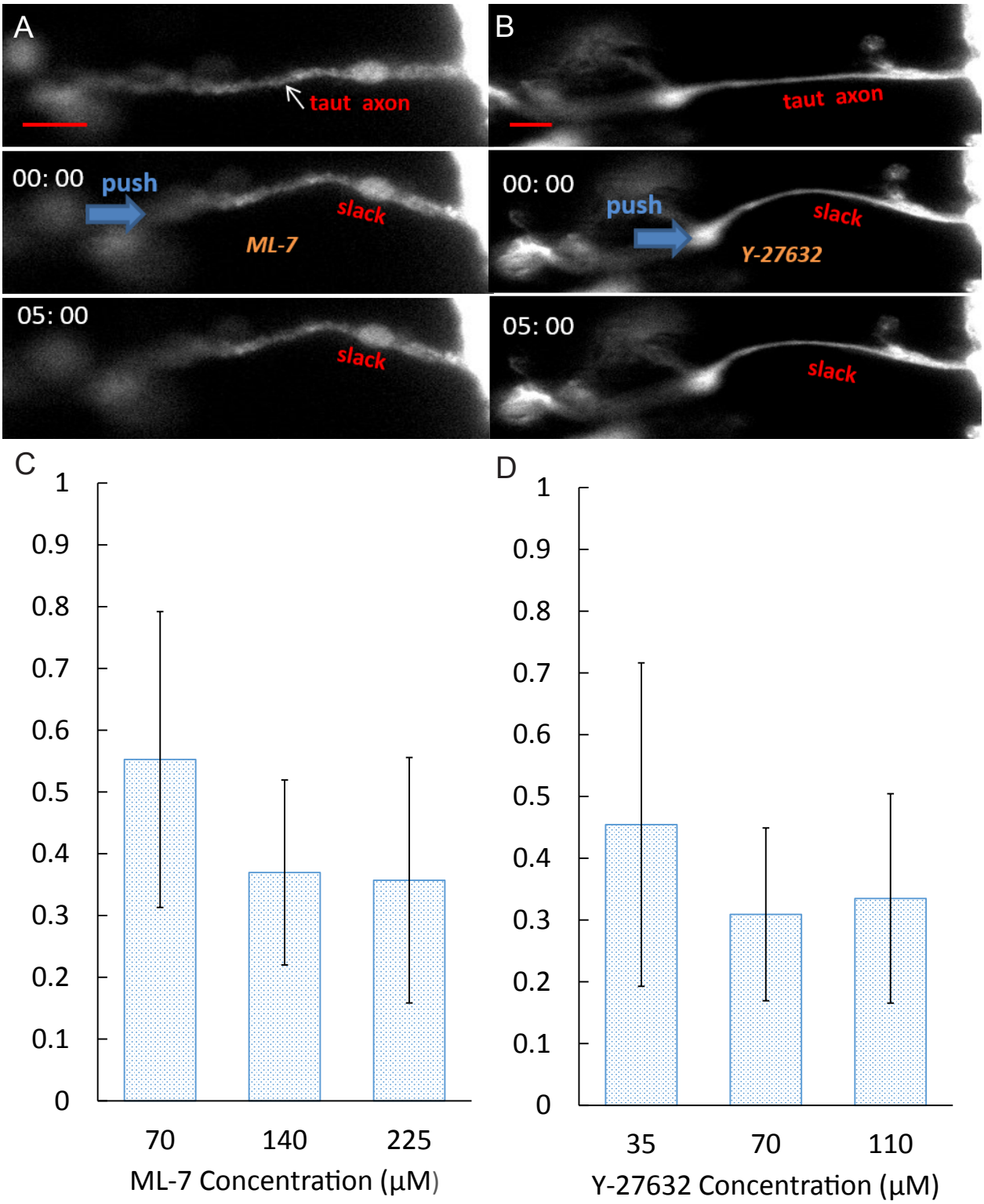

Figure S3: Axon contraction inhibited by ML-7 (A) and Y-27632 (B). Effect of ML-7 (C) and Y-27632 (D) at approximately 67% & 33% of the concentration reported in the main text. N=6 in all cases. All error bars in standard deviation. Note that ML-7 at the applied concentration may lead to the inhibition of PKA, PKC, and other pathways.

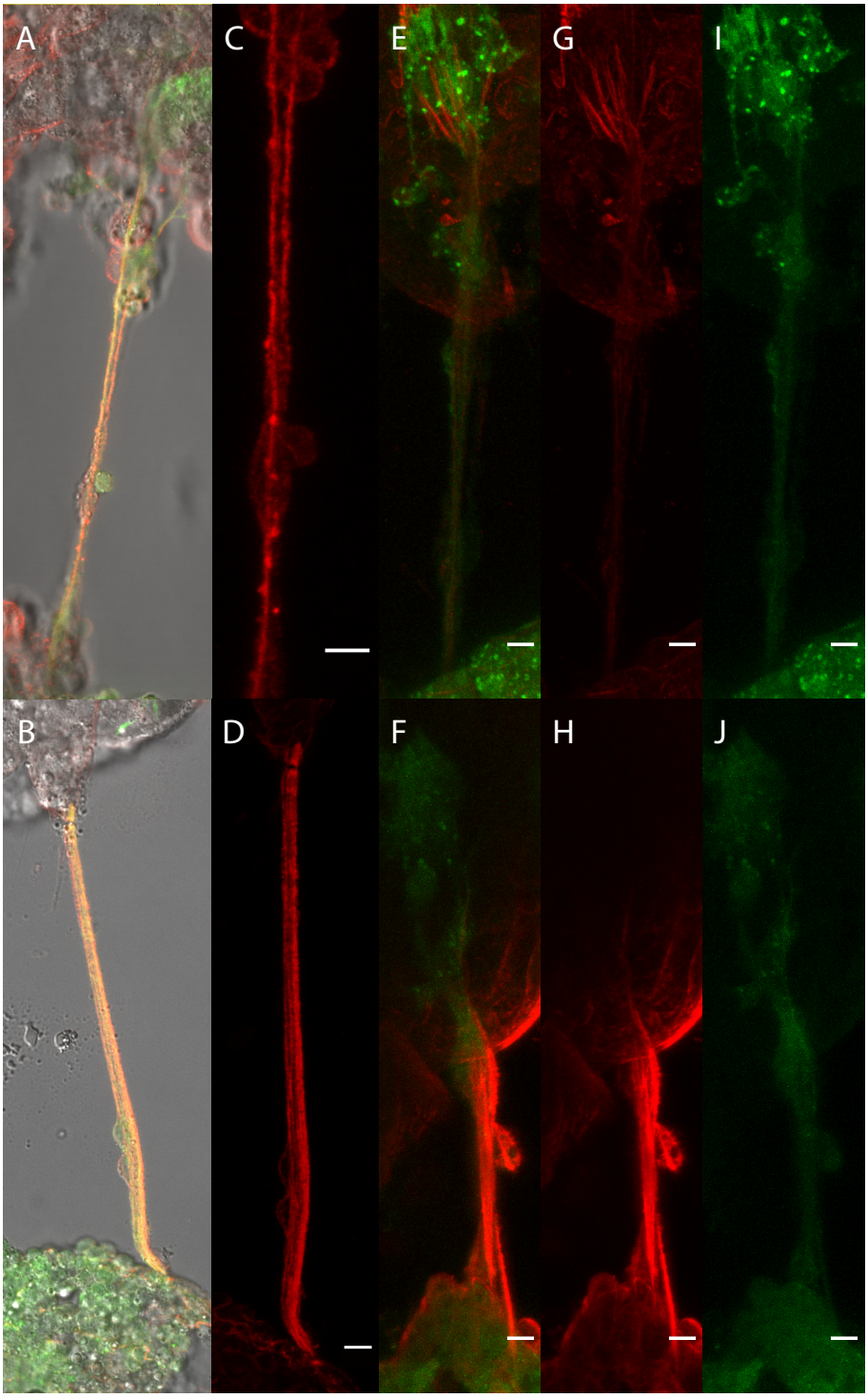

Figure S4: DIC, anti-α-tubulin, and neuronal-membrane-bound-GFP composite images with (A) and without (B) drug. Expanded images of microtubules morphology with (C) and without (D, reduced image gain by one-eighth due to saturation) drug. (E-J) Images obtained with a brief extraction step before fixation. Anti-α-tubulin and neuronal-membrane-bound-GFP composite images with (E, G, & I) and without (F, H, & J) drug. The composite images are separated into the two channels indicating the presence of polymerized microtubules (G & H) and neuronal membrane (I & J). Same imaging conditions applied unless otherwise noted.

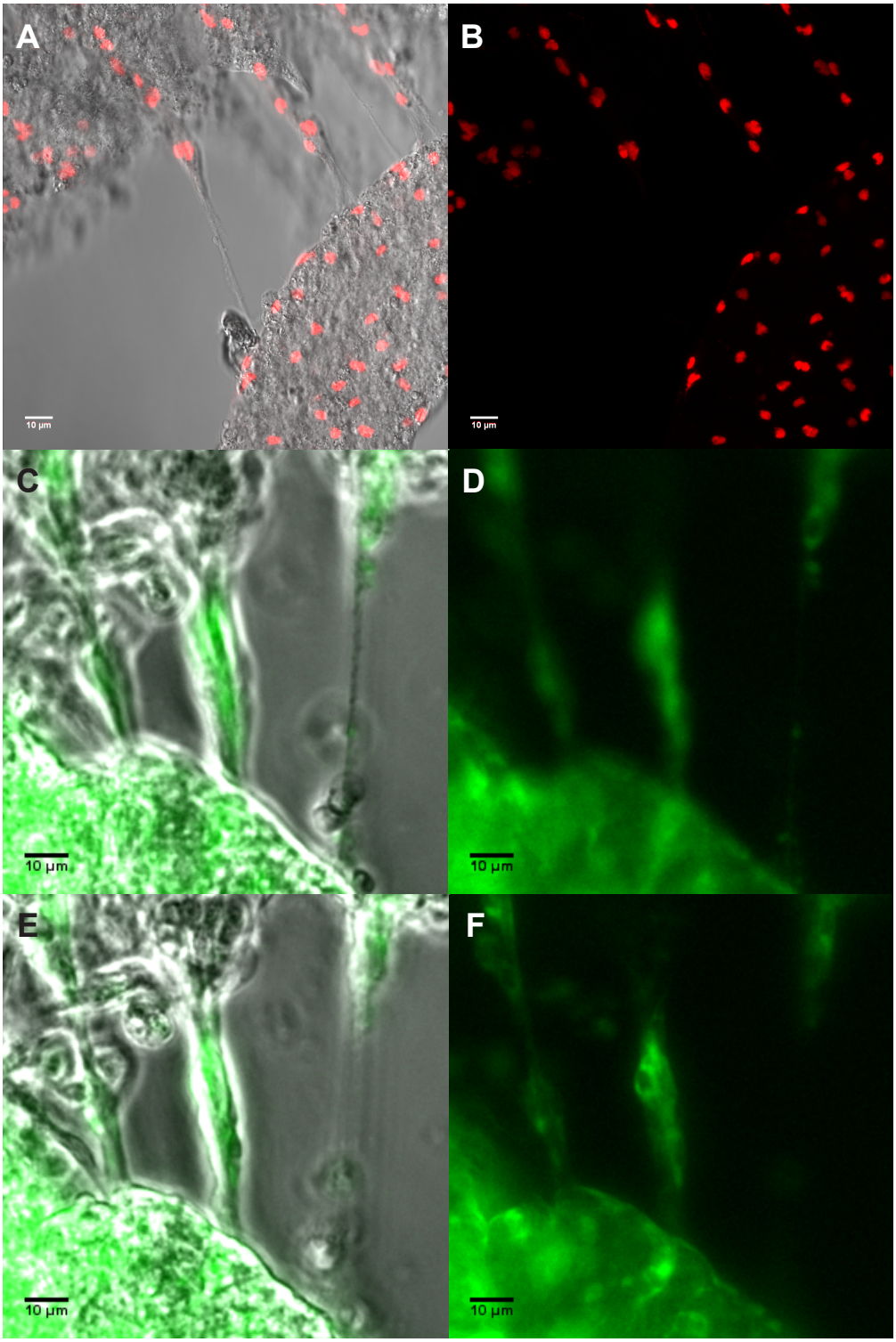

Figure S5: Glial cells visualizations, through staining (A-B) and crossing (C-F), show high degree of glial ensheatment of uncleaned axon, and minimal ensheathment along the axon shaft of cleaned axon. (A) DIC and anti-repo composite image of preparation. Cleaned axon on the left. (B) Anti-repo channel of A. (C & E) Phase and glial-membrane-bound-GFP composite images at 2 different focal planes. Cleaned axon on the right. (D & F) Glial-membrane-bound-GFP channel of C & E respectively.